

# International Journal of Engineering Research and Development



DOI: 10.29137/ijerad.1620378

Volume:17 Issue:03 Pages:509-524 November/2025

Research Article

# Synchrophasor Estimation Based on Quadrature Amplitude Modulation Using Artificial Ecosystem Optimization Algorithm

Alperen Şengül 10, Çağrı Altıntaşı\* 2, 30

<sup>1</sup>Erzincan Binali Yildirim University, Institute of Science, 24100, Erzincan, Türkiye <sup>2</sup>Erzincan Binali Yildirim University, Department of Electrical and Electronics Engineering, 24100, Erzincan, Türkiye <sup>3</sup>İzmir Demokrasi University, Department of Electrical and Electronics Engineering, 35140, İzmir, Türkiye

**Received:** 15/01/2025 **Accepted:** 11/06/2025 **Published Online:** 15/11/2025

**Final Version:** 30/11/2025

#### Abstract

The need to monitor power quality and detect faults in the power grid has increased due to diverse generation sources and growing loads, which create supply-demand imbalances. Synchrophasor measurements are used to address these issues and assess system stability. This study proposes using Quadrature Amplitude Modulation (QAM) for synchrophasor measurement. Initially, the power signal's frequency is estimated using the Artificial Ecosystem Optimization (AEO) algorithm. This estimated frequency serves as a reference for the QAM method. The power signal is then decomposed into positive and negative components based on this frequency. A moving average filter, acting as a low-pass filter, is applied to remove high-frequency noise and retain components aligned with the estimated frequency. As a result, the amplitude and phase of the desired frequency component are extracted. The method's effectiveness is evaluated based on the IEEE Std. C37.118.1 for both M and P classes. Results show that the proposed approach achieves phasor estimation errors within the acceptable limits defined by the standard. Moreover, its performance at 80 dB SNR is compared with recent methods from literature, demonstrating its superiority in synchrophasor estimation, particularly under steady-state and harmonic conditions.

### Keywords

Quadrature amplitude modulation, Phasor, Rocof, Synchrophasor, Total vector error, Optimization

<sup>\*</sup> Corresponding Author: cagri.altintasi@idu.edu.tr

#### 1. Introduction

For ideal system conditions, the power signal must be at nominal frequency and in pure sinusoidal form during production, transmission, and distribution. The disruptive effects caused by renewable energy sources and nonlinear elements affect the quality of the power signal, therefore the system must be constantly monitored and controlled. Monitoring and control systems play an important role in ensuring that the power system maintains its stability under changing conditions and returns to operating conditions within specified standards by activating the necessary procedures in the event of a disruptive effect (İpek, 2008). For this purpose, Phasor measurement units, which are real-time, high-precision devices designed to measure the instantaneous magnitude, phase angle, and frequency values of voltage and current signals in the network, are designed. PMUs use time synchronization to tag each measurement at its corresponding instant. Electric utilities install PMUs in important substations to address protection and control issues (Schweitzer, 2010). In addition, the PMU can be used as a standalone physical unit or as a compact unit integrated with other physical devices such as relays (Benmouyal et al., 2004; Gurusinghe et al., 2012).

In the electrical grid, a phasor is a complex number that indicates the sinusoidal waves' phase angle and magnitude. In previous studies, various methods are suggested for synchrophasor estimation, including DFT-based algorithms (Belega and Dallet, 2009; Macii et al., 2012; Belega and Petri, 2013; Orallo, 2013; Romano and Paolone, 2014; Zhan et al., 2016), Taylor-Fourier transform, (TFT) (Zamora-Mendez at al., 2015), Kalman Filter (Wood et al., 1985; De La and Pedro, 1991; De La O Serna and Rodriguez-Maldonado, 2011; Liu, 2012; Ferrero et al., 2016), Least Squares (LS) method (De La O Serna, 2007; Premerlani et al., 2007; Das and Sidhu, 2013; Belega et al., 2015a; Belega et al., 2015b), Zero Crossing (Begovic, 1993; Moore et al., 1996), Wavelet Transform (WT) (Ren and Kezunovic, 2011) Phase-Locked Loop (De La O Serna, 2014). These methods also have certain drawbacks. In the Zero Crossing method, errors may occur when determining the zero-crossing points, especially in the presence of disturbances such as harmonics and noise. Additionally, since the zero-crossing points can only be determined after the earliest half-cycle is defined, the method may be slow in detecting frequency changes (Gokoğlu,2019). While the DFT and its variant methods allow direct calculation, their performance decreases significantly for non-stationary and dynamic signals or when the signal deviates from its nominal value (Jin and Zhang, 2021). Although TFT-based methods are better than DFT on dynamic signals, they have lower estimation performance, especially on harmonic signals (Song et al., 2022; Fu et. al., 2021). The major disadvantages of the KF and LS methods are that they are difficult to apply to non-stationary and harmonic signals due to the high complexity and show poor performance in noisy environments (Song et al., 2022). The WT method, which utilizes a multi-stage low-pass filtering system within its cycle, introduces delays in the analysis process (Gokoğlu,2019).

# 1.1. Contribution of the study

This study presents a comprehensive performance analysis of P-class and M-class systems as defined in the IEEE Std. C37.118.1 standard, with the aim of achieving higher accuracy in synchrophasor measurements and mitigating the potential negative impacts mentioned above. To begin with, the Artificial Ecosystem algorithm (AEO) is employed to accurately estimate the fundamental frequency of the input signal. Once the frequency is determined, the signal is decomposed into its positive and negative sequence components through the application of the Quadrature Amplitude Method (QAM), which effectively separates the symmetrical components. Subsequently, to extract the instantaneous voltage-phase information relevant to the estimated frequency component, a moving average filter functioning as a low-pass filter (LPF) is applied. This filtering process attenuates high-frequency noise and isolates the desired signal features. The entire proposed methodology is implemented and tested in a simulation environment using MATLAB software, strictly adhering to the performance criteria outlined for both steady-state and dynamic conditions in IEEE Std. C37.118.1. Simulation results indicate that the developed approach successfully meets the precision and accuracy requirements specified for synchrophasor measurements in both P-class and M-class categories. In addition, the performance of the algorithm is tested at 80dB SNR noise and compared with the methods proposed in the literature in recent years. The findings indicate that the proposed method remains well within the upper bounds prescribed by the IEEE Std. C37.118.1 for synchrophasor estimation under all examined conditions, and exhibits markedly superior performance compared to existing approaches, particularly in steady-state and harmonic distortion cases.

## Symbols and Abbreviations

A	Ampere
k <sub>x</sub>	Amplitude Modulation Coefficient
ω	Angular Frequency
F	Frequency
$R_{\rm f}$	Frequency Rate
Hz	Hertz
ms	Millisecond
$f_{m}$	Modulation Frequency
φ	Phase Angle
ka	Phase Angle Modulation Coefficient
X'i	Predicted Factor Imaginary Part

 $X'_r$  Predicted Factor Real Part  $X_q$  QAM Negative Component  $X_d$  QAM Positive Component

 $\begin{array}{ccc} f_s & & Reporting \ Rate \\ s & Second \end{array}$ 

X<sub>m</sub> Signal Amplitude Value

 $X_1, X_2 \text{ ve } X_3$  Test Signals for Phase 1, 2, and 3 Theoretical Factor Imaginary Part  $X_r$  Theoretical Factor Real Part

t Time V Volt

ADC Analog Digital Converter

AEO Artificial Ecosystem-based Optimization

DFT Discrete Fourier Transform

FE Frequency Error

GPS Global Positioning System

IEEE Institute of Electrical and Electronics Engineers

KF Kalman Filter LPF Low Pass Filter

PMU Phasor Measurement Unit

QAM Quadrature Amplitude Modulation

RFE ROCOF Error

ROCOF Rate of Change of Frequency

SNR | Signal to Noise Ratio

Std. Standard

 $\begin{array}{lll} TFT & Taylor-Fourier\ transform \\ TVE & Total\ Vector\ Error \\ WT & Wavelet\ Transform \\ R_f & ROCOF\ (Hz/s) \end{array}$ 

# 2. Theoretical Foundations

The fundamental concepts to be used in the study, such as Phasor, ROCOF, and TVE, are discussed under this section. The phasor originated in the late 19th century by C. Proteus STEINTMETZ, inspired by Oliver HEAVISIDE's operational calculus (Robbins, 2012). A formulation that includes the amplitude and phase information of a sinusoidal signal is called a phasor representation.

The phasor representation of alternating current is given between Equation (1) and Equation (5) using Euler's identity;

$$V(t) = V_m \cdot \cos(wt + \alpha) \tag{1}$$

$$V(t) = V_m \cdot \cos(2 \cdot \pi \cdot f_0 \cdot t + \alpha) \tag{2}$$

Euler's Theorem:

$$e^{\pm j\alpha} = \cos(\alpha) \pm j.\sin(\alpha) \tag{3}$$

$$cos(\alpha) = Re(e^{j\alpha}), sin(\alpha) = Im(e^{j\alpha})$$
 (4)

$$V = V_m \cdot e^{j(2.\pi \cdot f \cdot t + \alpha)} = V_m \angle \alpha \tag{5}$$

The ROCOF is expressed as the derivative of the grid frequency with respect to time. The frequency in the electrical grid can vary depending on conditions such as imbalances between consumption and generation. ROCOF measures the rate of these frequency changes and is considered an important parameter in assessing the quality of power systems. For a signal given by Equation (6)

$$x(t) = X_m \cos(\vartheta(t)) \tag{6}$$

The frequency value is defined as given in Equation (7).

$$f(t) = \frac{1}{2\pi} \frac{d(\vartheta(t))}{dt} \tag{7}$$

In this case, ROCOF is measured in Hz/s and can be expressed as given in Equation (8).

$$ROCOF(t) = \frac{df(t)}{dt}$$
 (8)

The FE is defined as given in Equation (9).

$$FE = |f_{real} - f_{estimated}| \tag{9}$$

The *RFE* is defined as given in Equation (10).

$$RFE = |(df/dt)_{real} - (df/dt)_{estimated}|$$
(10)

Here, the real and estimated values are calculated for the values that have the same timestamp provided by the time source. The TVE represents the percentage difference between the estimated phasor values and the actual phasor value. This difference is commonly used as an error metric and helps in evaluating the accuracy of the computation method. The calculation for this is expressed as given in Equation (11).

$$TVE = \sqrt{\frac{\left(\left(X'_{r}(n) - X_{r}(n)\right)\right)^{2} + \left(\left(X'_{i}(n) - X_{i}(n)\right)\right)^{2}}{X_{r}(n)^{2} + X_{i}(n)^{2}}}$$
(11)

Here,  $X_r$  and  $X_i$  represent the real and imaginary components of the actual phasor values, while  $X'_r$  and  $X'_i$  denote the estimated phasor values resulting from the computations.

### 1.2. Defined standards for phasor measurement units

For synchrophasors, the IEEE 1344 standard was initially defined in 1995 and is reaffirmed in 2001. This standard defines the parameters of synchrophasors, including year, time quality, daylight saving time applications, and local time differences. In 2005, this standard is replaced by a complete revision, IEEE C37.118-2005, which addressed the use of PMUs in electric power systems (Zhang et al., 2007). In 2011, a new version is published that split the IEEE C37.118-2005 standard into two parts: C37.118-1 and C37.118-2. In 2014, a modification to C37.118.1 is published, replacing it with IEEE C37.118.1a-2014.

The reporting rate is determined by the PMU designer. For 50 Hz systems, options include 10, 25, and 50 samples per second, while for 60 Hz systems, options include 10, 12, 15, 20, 30, and 60 samples per second. Higher reporting rates, such as 100/s and 120/s, are also supported, while lower reporting rates, such as 1/s, are permitted. For designs with reporting rates less than 10/s, there is no requirement to meet the dynamic conditions specified in IEEE C37.118.1-2011.

# 1.3. Steady state test requirements

The FE, TVE, and ROCOF values calculated for steady-state conditions represent the scenario where the values of  $X_m$ ,  $\omega$ , and  $\phi$  are held constant throughout the test period. Steady-state tests are performed with frequency deviation, harmonic distortion, and out-of-band interference tests. The standard requirements for these tests are provided in Table 1, Table 2, and Table 3.

Table 1. Steady State Synchrophasor Measurement Requirements

		P Class			M Class			
Reference condition	Range	TVE <sub>max</sub>	$FE_{max}$	ROCOF <sub>max</sub>	Range	$TVE_{max}$	$FE_{max}$	ROCOF <sub>max</sub>
Nominal system	± 2 Hz	1	0.005	0.4	$f_s < 10$ for $\pm 2$ Hz	1	0.005	0.1
frequency					$10 \le f_s \le 25 \text{ for } \pm f_s/5$			
					$f_s \ge 25$ for $\pm 5$ Hz			

**Table 2**. Synchrophasor Measurement Bandwidth Requirements

P Class				M C	lass		
Range	$TVE_{max}$	$FE_{max}$	$ROCOF_{max}$	Range	$TVE_{max}$	$FE_{max}$	$ROCOF_{max}$
-	-	-	-	10% of input signal magnitude for $f_s \ge 10$	1.3	0.01	1.57
				No requirement for $f_s < 10$			

Table 3. Steady State Synchrophasor Harmonic Distortion Measurement Requirements

P	P Class				M Class			
Range	$TVE_{max}$	$FE_{max}$	$ROCOF_{max}$	Range	$TVE_{max}$	$FE_{max}$	ROCOF <sub>max</sub>	
	(%)	(Hz)	(Hz/s)		(%)	(Hz)	(Hz/s)	
1%, each harmonic up to	1	0,005	0,4	10%, each harmonic up to	1	0,005	7,85	
$50$ th ( $f_s \le 20$ )				$50$ th ( $f_s \le 20$ )				

# 1.4. Dynamic compliance-measurement bandwidth

This test is performed by modulating the amplitude and phase angle of the signal. The input test signals are given by Equation (12), Equation (13), and Equation (14).

$$X_1 = V_m[1 + k_x \cos(wt)] * \cos[w_0 t + k_a \cos(wt - \pi)]$$
(12)

$$X_2 = V_m [1 + k_x \cos(wt)] * \cos\left[w_0 t - \frac{2\pi}{3} + k_a \cos(wt - \pi)\right]$$
 (13)

$$X_3 = V_m[1 + k_x \cos(wt)] * \cos\left[w_0 t + \frac{2\pi}{3} + k_a \cos(wt - \pi)\right]$$
 (14)

Here,  $X_1$ ,  $X_2$  and  $X_3$  represent the phase signals for the three-phase system,  $w_0$  denotes the nominal angular frequency,  $w_0$  represents the modulation angular frequency,  $k_x$  is the amplitude modulation factor, and  $k_a$  is the modulation factor for the phase angle. For this test, the frequency at reporting times t=nT in the input signals defined above is expressed by Equation (15). The standard requirements for this test are presented in Table 4.

$$f(t) = \frac{w_0}{2\pi} - k_a \left(\frac{w}{2\pi}\right) \sin(wnT - \pi) \tag{15}$$

Table 4. Synchrophasor Measurement Requirements Using Modulated Test Signals

			P Cla	SS			МС	Class	
Level	Reference Condition	Range	TVE <sub>max</sub> (%)	FE <sub>max</sub> (Hz)	ROCOF <sub>max</sub> (Hz/s)	Range	TVE <sub>max</sub> (%)	FE <sub>max</sub> (Hz)	ROCOF <sub>max</sub> (Hz/s)
k <sub>x</sub> =0,1 k <sub>a</sub> =0	100% rated signal	$f_m$ : 0.1 to lesser of	3	0,03	0,06	$f_m$ : 0.1 to	3	0,12	2,3
$k_x=0$ $k_a=0,1$	magnitude, nominal system frequency	$f_s/10$ or 2 Hz	3	0,03	0,06	or 5 Hz	3	0,12	2,3

## 1.5. Dynamic compliance-performance during ramp of system frequency

In a power system, frequency can vary due to supply-demand imbalances and system failures. This test is performed by applying a linear slope test to the system frequency. For the method proposed in this study, the frequency ramp test conditions could not be met. The input test signals are given by Equation (16), Equation (17) and Equation (18).

$$X_1 = V_m * cos[w_0 t + \pi R_f t^2]$$
 (16)

$$X_2 = V_m * cos \left[ w_0 t - \frac{2\pi}{3} + \pi R_f t^2 \right]$$
 (17)

$$X_3 = V_m * cos \left[ w_0 t + \frac{2\pi}{3} + \pi R_f t^2 \right]$$
 (18)

For this test, the frequency at reporting times t=nT in the input signals defined above is expressed as given in Equation (19). The standard requirements for this test are presented in Table 5.

$$f(t) = f_0 + R_f \left( t - \frac{\Delta t}{2} \right) \tag{19}$$

**Table 5.** Synchrophasor Performance Requirements under Frequency Ramp Tests

P Class						M	Class	
ROCOF Rf (Hz/s)	Range	FEmax (Hz)	TVEmax (%)	ROCOFmax (Hz/s)	Range	FEmax (Hz)	TVEmax (%)	ROCOFmax (Hz/s)
± 1 Hz/s	± 2 Hz	0,01	1	0,4	Lesser of $f_s$ /5 Hz or $\pm$ 5 Hz	0,01	1	0,2

### 1.6. Dynamic compliance-performance under step changes in phase and magnitude

This test is performed by applying a step change to the amplitude and phase angle of the signal starting from a certain time. The input test signals are given by Equation (20), Equation (21), and Equation (22).

$$X_1 = V_m [1 + k_x f_1(t)] * \cos[w_0 t + k_a f_1(t)]$$
(20)

$$X_2 = V_m[1 + k_x f_1(t)] * cos \left[ w_0 t - \frac{2\pi}{3} + k_a f_1(t) \right]$$
 (21)

$$X_3 = V_m[1 + k_x f_1(t)] * \cos\left[w_0 t + \frac{2\pi}{3} + k_a f_1(t)\right]$$
 (22)

The standard requirements for this test are presented in Table 6 and Table 7. The measurement response time refers to the time difference between the moment before and after a step change is applied to an input signal and the point at which steady-state is reached. The delay time is the time interval between the application of a step change to the PMU input and the achievement of the initial and final steady-state values of the step parameter (Gokoglu, 2019).

Table 6. Phasor Performance Requirements for Input Step Change

	Tuble	P Class	mance Requirement	s for input step	M Class	
Modulation level	Response time (s)	Delay time  (s)	Max overshoot/ undershoot	Response time (s)	Delay time  (s)	Max overshoot/ undershoot
Magnitude±10% k <sub>x</sub> =0,1, k <sub>a</sub> =0	$2/f_0$	1/(4.f <sub>s</sub> )	%5 of step	$7/f_{\rm s}$	1/(4.f <sub>s</sub> )	%10 of step
Angle±10% k <sub>x</sub> =0, k <sub>a</sub> =0,1			magnitude			magnitude

 Table 7. Frequency and ROCOF Performance Requirements for Input Step Change

	P C	lass	M Class		
Modulation level	Frequency	ROCOF	Frequency	ROCOF	
	response time (s)	response time (s)	response time (s)	response time (s)	
$\begin{array}{c} \text{Magnitude}{\pm 10\%} \\ \text{$k_x$=}0.1 \text{ $k_a$=}0 \\ \text{Angle}{\pm 10\%} \\ \text{$k_x$=}0, \text{$k_a$=}0,1 \end{array}$	$4.5/f_0$	6/f <sub>0</sub>	Greater of $14/f_s$ or $14/f_0$	Greater of $14/f_s$ or $14/f_0$	

# 2. Materials and Methods

In this study, the proposed method for the synchrophasor measurement process consists of three steps. The frequency of the measured signal is first estimated by the AEO algorithm. The power signal is then decomposed into its positive and negative components at the estimated frequency using QAM. These components are subsequently passed through a low-pass moving average filter, which removes the high-frequency components, leaving only the components corresponding to the desired frequency. In this way, the FE, TVE, and ROCOF values are calculated depending on the instantaneous amplitude and phase angle for the synchrophasor. The block diagram

for these processes is shown in Figure 1. Each step of the proposed method is explained in detail below. GPS is used to provide an accurate time reference to all measurement devices and for common time tagging.

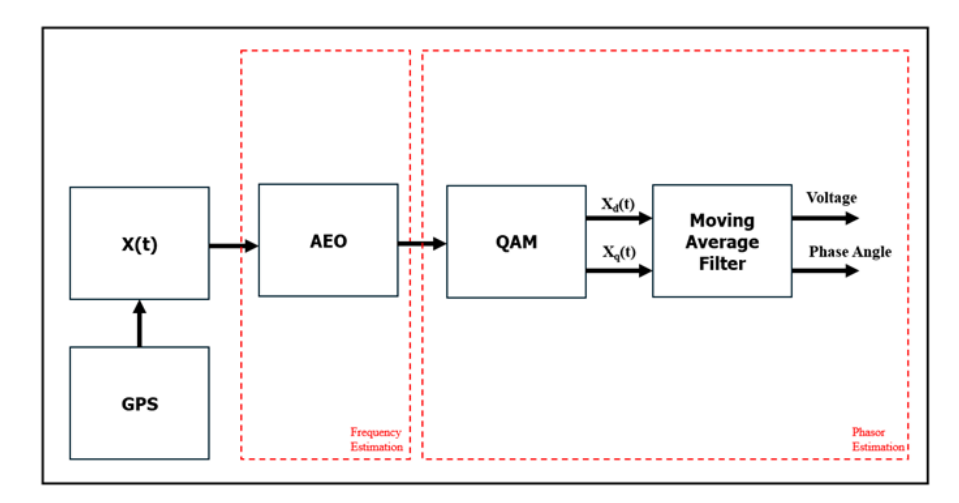


Figure 1. Amplitude and Phase Angle Calculation with OAM Block Diagram.

#### 2.1. Artificial ecosystem-based optimization algorithm

AEO is an optimization algorithm inspired by biological ecosystems and consists of production, consumption and decomposition sections. This algorithm searches for potential solutions within the solution space. The first step involves generating an initial population with random values within the solution space by determining the maximum number of iterations and population size. An environmental model is created based on the problem's constraints and objectives, and the performance of the solutions is evaluated. The solution candidates within the population are classified based on their quality, and selection of the candidates is carried out.

The definitions and mathematical expressions for this algorithm are provided below (Zhao et al., 2020). The mathematical expression for the production stage of the algorithm is given by Equation (23).

$$X_1(t+1) = (1-a)X_n(t) + aX_{rand}(t)$$
(23)

$$a = \left(\frac{1-t}{T}\right)r_1\tag{24}$$

$$X_{rand} = r * (up - lw) + lw (25)$$

Where, T is the maximum number of iterations, t denotes the current iteration value,  $r_l$  is a random number between [0, 1], a is a coefficient used for linear weighting, n is the number of populations, r is a random vector whose elements are in the interval [0, 1] and up and lw are upper and lower boundaries, respectively.

The terms  $X_i$ ,  $X_n$ , and  $X_j$  represent the solution vectors in the algorithm. In the algorithm, these terms generally refer to the individuals (population members) or solution points within the solution search process. r is a random vector whose elements are in the interval [0, 1]. This term is commonly used in algorithms to simulate randomness. up and lw represent the maximum and minimum values that each component of the solution can take. In other words, they define the boundaries for each component of the solution vector that the algorithm seeks. i and n are indices of the individuals within the population. i typically refers to a specific individual (population element), while n denotes the total number of individuals in the population. Thus, n represents the size of the entire population in the algorithm, and i refers to a particular individual within that population. The mathematical expression for the consumption stage is given by Equation (26).

$$X_i(t+1) = X_i(t) + C[X_i(t) - X_1(t)], i \in [2,..,n]$$
(26)

$$C = \left(\frac{1}{2}\right)(v_1/v_2), \qquad v_1, \ v_2 \sim N(0,1)$$
 (27)

where, N(0,1) represents a normal distribution.

$$X_i(t+1) = X_i(t) + C[X_i(t) - X_i(t)]$$
(28)

Here,  $i \in [3,...,n]$  and  $j \in [2 \text{ i-1}]$  take random integer values.

$$X_i(t+1) = X_i(t) + C[r_2(X_i(t) - X_1(t)) + (1 - r_2)(X_i(t) - X_j(t))]$$
(29)

The mathematical model of the decomposition part of the algorithm is obtained as shown in Equation (30).

$$X_i(t+1) = X_n(t) + D[eX_n(t) - hX_i(t)], i \in [1, n]$$
(30)

Here, D=3u, where  $u \sim N(0,1)$ ,  $e=r_3 randi([1\ 2]-1)$ ,  $h=2r_3-1$  and  $r_2,r_3$  are random values between  $\theta$  and I.

In this study, the objective function for frequency estimation is defined in Equation (31) as minimizing the RMS error of the estimated signal ( $x_{estimated}$ ) with the actual signal ( $x_{actual}$ ).  $x_{actual}$  represents each case for the synchrophasor measurement defined in subsections 2.2 to 2.5.  $\hat{V}$ ,  $\hat{f}_0$ , and  $\hat{\alpha}$  in  $x_{estimated}$  are the parameters to be estimated.

$$J = min \sqrt{\frac{1}{N} \sum_{k=1}^{N} (x_{actual} - x_{estimated})^2} , \qquad x_{estimated} = \hat{V}\cos(2\pi \hat{f_0} t + \hat{\alpha})$$
 (31)

Flow chart diagram for AEO is provided in Figure 2. It begins with the initialization of essential parameters such as population size, iteration limit, and variable boundaries. An initial population of candidate solutions is then generated, and their fitness is evaluated using a defined objective function. The best individual is identified and stored. The algorithm then enters an iterative loop based on the randomly assigned  $r_1$  value. After these steps, the population is updated, fitness is re-evaluated, and the best solution is continually tracked. This loop continues until the maximum number of iterations is reached, after which the algorithm returns the best solution found.

## 2.2. Quadrature amplitude modulation

QAM is the process of modulating a message signal with carrier signals. This technique enables the transmission of the signal by shifting the frequency components of the message signal to the carrier signal frequency. When the message signal is multiplied by the carrier signals, high and low-frequency components are generated. The low-frequency component appears at 0 Hz as a result of modulation, while the high-frequency component appears at twice the fundamental frequency. Thus, data related to signals formed around 0 Hz can be obtained by using a low-pass filter. This method allows the extraction of instantaneous amplitude and phase angle data at the frequencies contained in the signal. In this method, the message signal is modulated with two carrier signals that have a phase difference of 90° between them.

As expressed by Equation (32), an X(t) current or voltage signal with amplitude A, fundamental frequency  $f_{\theta}$  and phase angle  $\varphi$  is generated:

$$X(t) = A\cos(2\pi f_0 t + \varphi) \tag{32}$$

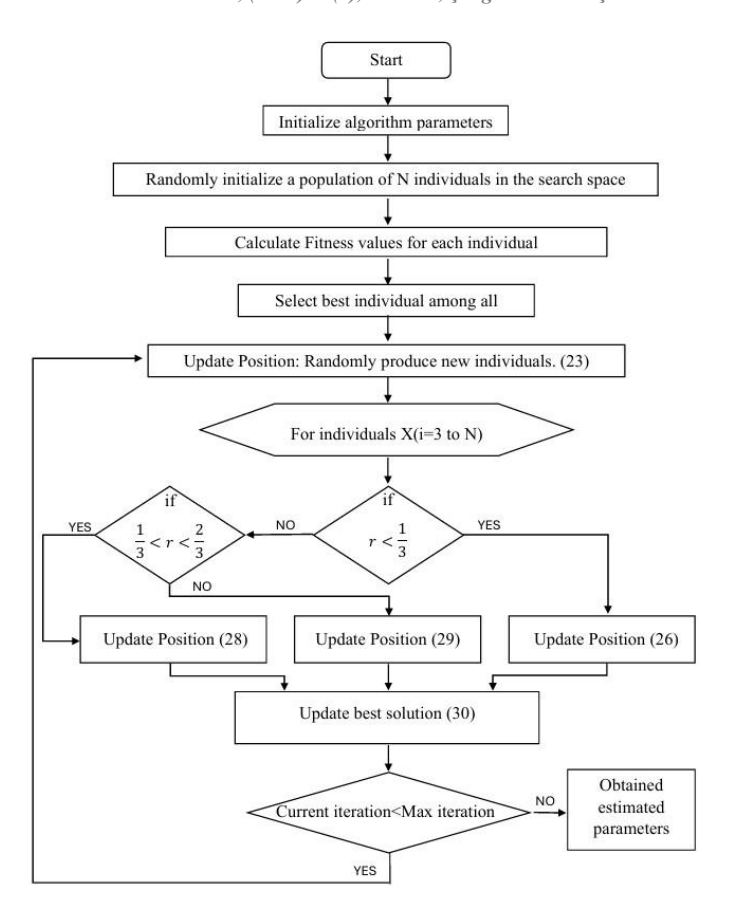


Figure 2. Flow Chart of the AEO

In the QAM method, to generate the carrier signals, the X(t) signal expressed by Equation (32) is multiplied by  $e^{jwt}$  and as shown in Equations (33) and (34), the real and imaginary components are formed. Here,  $X_m(t)$  represents the modulated signal, and  $f_m$  represents the modulation frequency.

$$e^{j2\pi f_m t} = \cos(2\pi f_m t) + j\sin(2\pi f_m t) \tag{33}$$

$$X_m(t) = \left(A\cos(2\pi f_0 t + \varphi)\right) * \left(\cos(2\pi f_m t) + j\sin(2\pi f_m t)\right)$$
(34)

The real and imaginary parts are expressed with Equations (35) and (36).

$$Re(X_m(t)) = (A\cos(2\pi f_0 t + \varphi)) * (\cos(2\pi f_m t))$$
(35)

$$Im(X_m(t)) = (Acos(2\pi f_0 t + \varphi)) * (sin(2\pi f_m t))$$
(36)

The real and imaginary components can be expressed using the inverse transformation formulas of trigonometric functions, as shown in Equations (37) and (38).

$$Re(X_m(t)) = \frac{A}{2} * \left[ \left( \cos(2\pi(f_0 + f_m)t + \varphi) \right) + \left( \cos(2\pi(f_0 - f_m)t + \varphi) \right) \right]$$
(37)

$$Im(X_m(t)) = \frac{A}{2} * \left[ \left( sin(2\pi(f_0 + f_m)t + \varphi) \right) + \left( sin(2\pi(f_0 - f_m)t + \varphi) \right) \right]$$
(38)

When the modulation signal  $f_m$  is chosen to be equal to the fundamental frequency  $f_0$  two components are formed: one at 0 Hz and the other at a higher frequency. To eliminate the high-frequency component, the signal is passed through a low-pass filter, resulting in the component formed around 0 Hz.

The real and imaginary components of the signal resulting from the filtering process can be expressed as shown in Equations (39) and (40).

$$Re(X_m(t)) = \frac{A}{2} * \left[ \left( \cos(2\pi (f_0 - f_m)t + \varphi) \right) \right]$$
(39)

$$Im(X_m(t)) = \frac{A}{2} * \left[ \left( sin(2\pi (f_0 - f_m)t + \varphi) \right) \right]$$

$$\tag{40}$$

To obtain the amplitude value of the signal, the squares of the components given in Equations (39) and (40) are summed, and their square roots are taken. To eliminate the reduction of the voltage value by half, which results from the trigonometric transformation formulas, the result is multiplied by 2. This is shown in Equation (41).

$$A = 2\sqrt{\left(Re\left(X_m(t)\right)^2 + Im\left(X_m(t)\right)^2\right)} \tag{41}$$

To obtain the phase angle of the signal, the components given in Equations (39) and (40) are ratioed and the inverse tangent value is taken. This is shown in Equation (42).

$$\varphi = tan^{-1} \frac{Im(X_m(t))}{Re(X_m(t))} \tag{42}$$

# 2.3. Moving average filter

A low-pass filter is used to suppress unwanted noise in the power signal. In this study, a moving average filter is utilized for the filtering process. The moving average filter is a signal processing technique used for smoothing a time series. This filter generates a new data point by averaging the data points over a specific window. This process reduces fluctuations in the data and provides a more regular appearance.

The general representation for the moving average filter is calculated as shown in Equation (43).

$$y[n] = \frac{1}{M} \sum_{m=0}^{M-1} x[n-m]$$
 (43)

The window length for the moving average filter refers to the number of samples contained within the sampling window used to calculate the average. For example, when a window size of 5 is chosen, each moving average value is calculated using a window that contains 5 samples, including the sample at that moment. The moving average value is obtained by averaging these samples. The window is then shifted one sample to the right, and the process is repeated.

# 3. Simulation Results

In this section, simulation results for the method used in the study are provided. For the synchrophasor measurement, steady-state and dynamic compliance tests as specified in the IEEE 37.118-2011 and IEEE 37.118-2014 standards are conducted. The computations are performed on a computer equipped with a Windows 10 operating system, an Intel processor running at 2.40 GHz, and 8 GB of RAM. Test signals are generated in the MATLAB environment, and samples are taken every 0.5 seconds for a data length of 5 seconds. The FE, TVE, and ROCOF values are calculated over 10 cycles. The reporting rate is 2 samples per second. The base frequency for the test signals is taken as 50 Hz, with a sampling frequency of 3200 samples per second. All voltage values are expressed in per unit (p.u.). For the AEO algorithm, the population size (number of particles) and the maximum number of iterations are set to 50 and 300, respectively. In (32), the lower limits of  $\hat{V}$ ,  $\hat{f}_0$ , and  $\hat{\alpha}$  to be estimated are 0.9 p.u., 44Hz, and - $\pi$ , while the upper limits are 1.1 p.u, 56Hz, and  $\pi$ .

#### 3.1. Steady state test results

Steady-state tests are conducted for frequency deviation and harmonic distortion tests.

## 3.1.1. Frequency deviation, amplitude and phase angle tests

The simulation results for frequency deviation, amplitude, and phase angle tests, based on the FE, TVE, and ROCOF requirement values provided in previous sections, are presented in Table 8, Table 9, and Table 10. The frequency test is conducted by varying the signal frequency between 48-52 Hz with 1 Hz steps. As a result, the highest error values measured are 4.98e-14 for FE, 8.63e-09 for TVE, and 1.27e-13 for ROCOF. The simulation results with respect to the number of cycles are shown in Figure 3.

Table 8. Simulation Results for Steady-State Frequency Test

Frequency	$FE_{max}$	$TVE_{max}$	ROCOF <sub>max</sub>
(Hz)	(Hz)	(%)	(Hz/s)
48	3.55e-14	7,53e-09	7,11e-14
49	4,26e-14	8,61e-09	8,52e-14
50	4,97e-14	8,63e-09	1,27e-13
51	4,26e-14	8,18e-09	7,10e-14
52	4,98e-14	7,60e-09	9,94e-14

**Table 9.** Simulation Results for Steady-State Amplitude Test

Amplitude Test	Range	TVE <sub>max</sub> (%)
Amplitude	Between 10% and 120% of the nominal	1,07e-08

Table 10. Simulation Results for Steady-State Phase Angle Test

Phase Angle Test	Range	$TVE_{max}$ (%)
Phase Angle	$\pm\pi$	1,64e-08

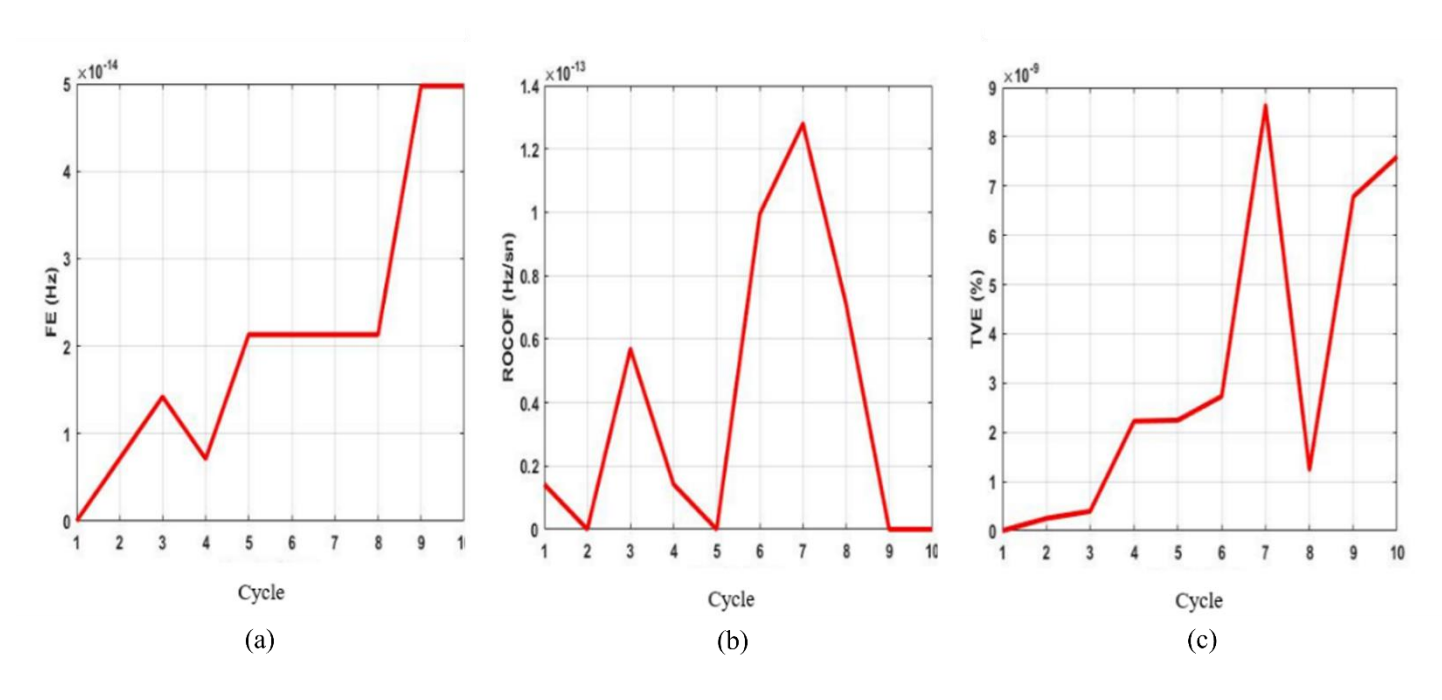


Figure 3. (a) Frequency Test Simulation Results FE; (b) ROCOF; (c) TVE.

The amplitude test is conducted by varying the signal amplitude within the range of 10% to 120% of the nominal amplitude value, with 1% steps. As a result, the highest error value for TVE is measured as 1.07e-08. The graphs of the measurement results with respect to the number of cycles are shown in Figure 4. The phase angle test is conducted by varying the signal phase angle within the range of  $\pm \pi$ , with 1° steps. As a result, the highest error value for TVE is measured as 1.64e-08.

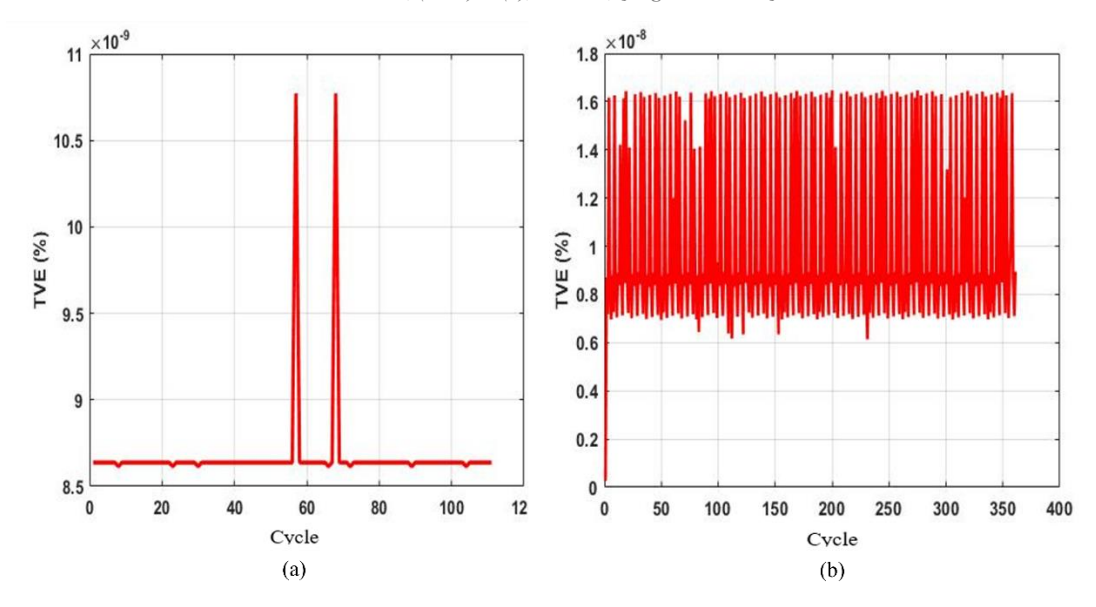


Figure 4. (a) TVE Simulation Results for Steady-State Amplitude Test; (b) Phase Angle Test.

#### 3.1.2. Harmonic distortion test

The harmonic distortion test is performed with a test signal containing components from the 2<sup>nd</sup> harmonic to the 50<sup>th</sup> harmonic. As a result, the highest error value for FE is measured as 2.86e-11, the highest error value for TVE is 4.97e-06, and the highest error value for ROCOF is 7.63e-11. The simulation results with respect to the number of cycles are provided in Table 11 The graphs for the specified test are provided in Figure 5.

Table 11. Harmonic Distortion Test Results							
Harmonic distortion	FE	TVE	ROCOF				
Harmonic distortion	(Hz)	(%)	(Hz/s)				
10%, each harmonic up to 50th	2,86e-11	8,02e-06	9,98e-11				

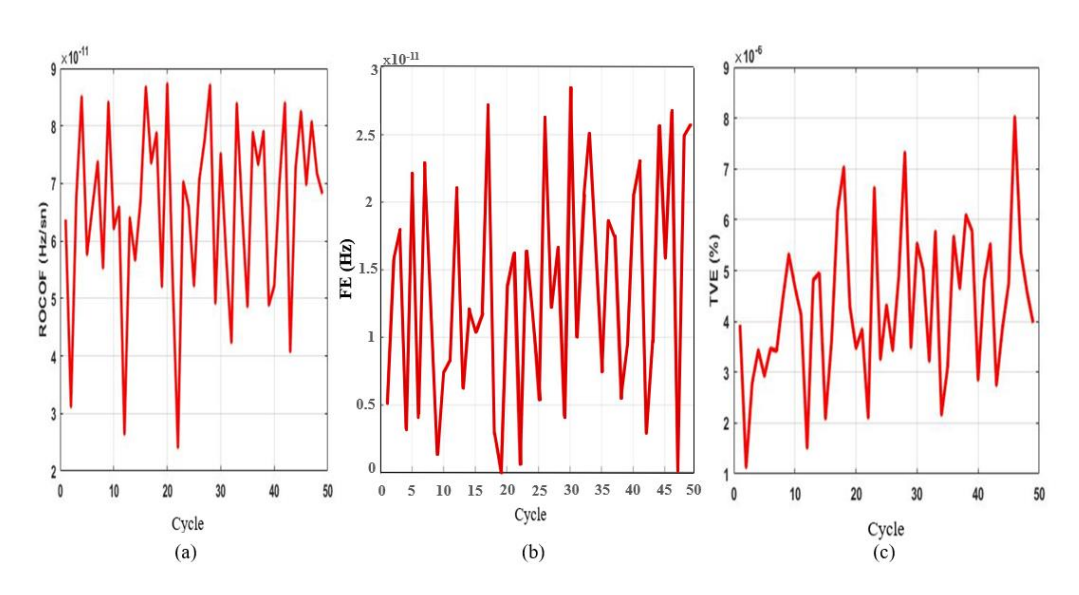


Figure 5. (a) Harmonic Distortion Test Simulation Results ROCOF; (b) FE; (c) TVE.

# 3.2. Dynamic compliance-measurement bandwidth test results

This test is conducted by modulating the signal's amplitude and phase angle. In the amplitude and phase modulation, the modulation frequency is changed within the range of 0.1 to  $f_s/5$  with steps of 0.1 Hz. As a result, the highest error value for FE is measured as 0.023, for TVE as 0.71, and for ROCOF as 0.0029. The simulation results for the measurement according to the number of cycles are presented in Table 12.

Table 12. Measurement Bandwidth Test Results

Table 12. Weasarement Bandwidth Test Results							
Measurement bandwidth test	Range	FE	TVE	ROCOF			
		(Hz)	(%)	(Hz/s)			
$k_x = 0,1 k_a = 0$	_	1,19e-04	0,71	2,68e-04			
$k_x = -0.1 k_a = 0$	$f_m:0.1-f_s/5$	1,27e-04	0,59	1,66e-04			
$k_x=0, k_a=0,1$	_	0,023	0,65	0,0029			
$k_x=0, k_a=-0,1$	-	0,022	0,64	0,0028			

The simulation results for the test are presented in Figure 6.

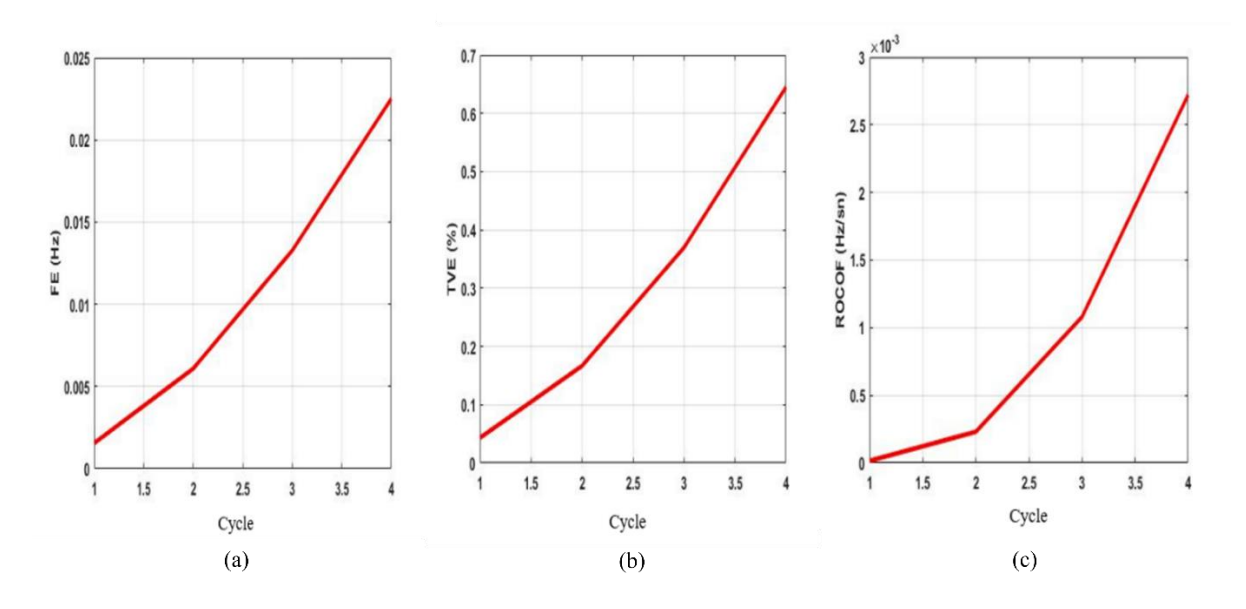


Figure 6. Measurement Bandwidth Simulation Graphs (a) FE; (b) TVE; (c) ROCOF.

### 3.3. Dynamic compliance-performance under step changes in phase and magnitude test results

This test involves applying positive and negative step signals with 10% amplitude and 10% phase angle magnitude to the input signal. A unit step function is applied to the function at a specific moment, and the performance is measured in response to the sudden input change. A unit step function is applied to the input signal starting from t = 0.5 seconds. The simulation results are provided in Table 13.

Table 13. Step Changes in Phase and Magnitude Test Results

Step changes	Frequency response time (s)	TVE response time (s)	Delay time  (s)	Amplitude step change (%)
$k_x=10\%, k_a=0$	0	0,5083	0,0032	0,6
$k_x = -10\%, k_a = 0$	0	0,5763	0,0124	0,28
$k_a=10\%, k_x=0$	0,4694	0,6093	0,0022	0,11
$k_a = -10\%, k_x = 0$	0,513	0,6093	0,0076	0,5

## 4. Performance of Proposed Algorithm

The performance of the proposed method is tested by generating 80 dB SNR noise for all cases and compared with the i-IPDFT (Derviškadić, A et al., 2017), HM-ESPRIT (Drummond et al., 2020), and TLTFT (Shan et al., 2023) methods in the literature. The proposed algorithm is executed 10 times, and the best result among all runs is recorded and all data is provided in Table 14. Compared to existing approaches in the literature, the proposed method exhibits superior performance in Steady-State Frequency and Harmonic Distortion tests with respect to TVE, FE, and ROCOF metrics. Furthermore, it delivers improved ROCOF accuracy under Magnitude Modulation and Phase Modulation scenarios. Although the algorithm achieves better results than the TLTFT method in both magnitude and phase step response tests, its performance remains inferior to that of the other methods. The proposed method exhibits a performance reduction under off-nominal frequency conditions due to the inherent limitations of the low-pass filter. Nevertheless, the algorithm remains within the compliance thresholds defined by the IEEE Std. C37.118.1. Across all test cases, the average computation time required for synchrophasor estimation is approximately 0.56 seconds.

Table 14. Performance Comparison under 80 dB SNR Noise

Test Cases		Proposed	i-IPDFT		HM-ESPRIT	TLTFT
			Cos	Hann		
			Window	Window		
Steady-State Frequency	$TVE_{max}$ , (%)	1,27x10 <sup>-8</sup>	0,002	0,003	0,003	0,07
	$FE_{max}(Hz)$	$2,47x10^{-13}$	$10^{-4}$	$10^{-4}$	1,87x10 <sup>-4</sup>	$3 \times 10^{-4}$
	$ROCOF_{max}$ (Hz/s)	8,93x10 <sup>-12</sup>	0,009	0,012	0,023	0,07
Harmonic Distortion	$TVE_{max}$ , (%)	5.1x10 <sup>-6</sup>	0,047	0,003	0,004	0,1
	$FE_{max}(Hz)$	2.94x10 <sup>-11</sup>	$1,1x10^{-3}$	$10^{-4}$	1,98x10 <sup>-4</sup>	$1,6 \times 10^{-3}$
	$ROCOF_{max}$ (Hz/s)	7.79x10 <sup>-11</sup>	0,009	0,011	0,028	0,46
Magnituda	$TVE_{max}$ , (%)	0,62	0,847	0,604	0,021	0,06
Magnitude Modulation	$FE_{max}(Hz)$	1,36x10 <sup>-4</sup>	$1,6x10^{-3}$	$4x10^{-4}$	$6,92x10^{-4}$	$7 \times 10^{-3}$
Modulation	$ROCOF_{max}$ (Hz/s)	2,72x10 <sup>-4</sup>	0,051	0,0016	0,024	1,8
Phase	$TVE_{max}$ , (%)	0,66	0,806	0,547	0,139	0,05
Modulation	$FE_{max}(Hz)$	0,028	$22x10^{-3}$	$17,4x10^{-3}$	$36,2x10^{-3}$	$1,43 \times 10^{-4}$
Modulation	$ROCOF_{max}$ (Hz/s)	0,0031	0,683	0,540	4,758	1,5
Magnitude Step	Frequency response time (s)	0,4791	0,048	0,044	0,055	2,8
	TVE response time (s)	0,5843	0,034	0,028	0,018	0,9
	Delay time  (s)	0,0174	0,002	0,002	0,001	=
	Amplitude step change (%)	0,66	0	0	4,875	-
Phase Step	Frequency response time (s)	0,523	0,048	0,044	0,056	2,7
	TVE response time (s)	0,6193	0,04	0,032	0,023	1,3
	Delay time  (s)	0,0084	0,002	0,002	0,001	=
	Amplitude step change (%)	0,52	0	0	5,271	-

#### 5. Conclusion

Synchrophasors are crucial for maintaining power quality, efficiency, control, and protection schemes in electrical systems, and this work proposes a QAM-based technique to monitor them precisely and accurately. The moving average filter is a mathematically simple and easy to apply method. It smooths sudden changes in time series data, providing smoother and more analyzable data. However, increasing the window length can lead to a loss of resolution, so it is important to carefully select the window size. Additionally, it may perform poorly in detecting rapid changes, which can be a disadvantage in applications that require fast data changes, such as dynamic systems. The frequency component estimation for the input signals is performed using the AEO algorithm. FE, TVE, and ROCOF values are evaluated for compliance with mandatory requirements for the measured synchrophasors. Simulation results show the calculated data is well below the upper limit values specified in the relevant standards. This proves that the proposed method can calculate synchrophasors accurately and precisely. The IEEE C37.118.1 standards, which are used as the basis for synchrophasor measurement compliance, do not include tests for unbalanced loads, switching harmonics with high frequencies, electromagnetic interference, and transient states occurring in the system. In real-world conditions, the grid may be affected by all these factors. Therefore, PMUs and test standards are still open to development. Future studies can lead to the development of new algorithms and test standards. The robustness of the proposed method indicates that it can be applied to the signals that belong to different branchs of the network. Therefore, as a future work this method will be applied to real-time signals.

# 6. References

Begovic, M. M., Djuric, P. M., Dunlap, S., & Phadke, A. G. (1993). Frequency tracking in power networks in the presence of harmonics. IEEE Transactions on Power Delivery, 8(2), 480-486.

Belega, D., & Dallet, D. (2009). Multifrequency signal analysis by interpolated DFT method with maximum sidelobe decay windows. Measurement, 42(3), 420-426.

Belega, D., & Petri, D. (2013). Accuracy analysis of the multicycle synchrophasor estimator provided by the interpolated DFT algorithm. IEEE Transactions on Instrumentation and Measurement, 62(5), 942-953.

Belega, D., Fontanelli, D., & Petri, D. (2015). Low-complexity least-squares dynamic synchrophasor estimation based on the discrete Fourier transform. IEEE Transactions on instrumentation and Measurement, 64(12), 3284-3296.

Belega, D., Fontanelli, D., & Petri, D. (2015). Dynamic phasor and frequency measurements by an improved Taylor weighted least squares algorithm. IEEE Transactions on Instrumentation and Measurement, 64(8), 2165-2178.

Benmouyal, G., Schweitzer, E. O., & Guzman, A., Synchronized phasor measurement in protective relays for protection, control, and analysis of electric power systems, 57th Annual Conference for Protective Relay Engineers, 2004, USA, 2004, pp. 419-450.

Das, S., & Sidhu, T. (2013). A simple synchrophasor estimation algorithm considering IEEE standard C37. 118.1-2011 and protection requirements. IEEE Transactions on Instrumentation and Measurement, 62(10), 2704-2715.

De la O Serna, J. A. (2007). Dynamic phasor estimates for power system oscillations. IEEE Transactions on Instrumentation and Measurement, 56(5), 1648-1657.

De la O Serna, J. A., & Rodriguez-Maldonado, J. (2011). Instantaneous Oscillating Phasor Estimates With Taylor \$^ K \$-Kalman Filters. IEEE Transactions on Power Systems, 26(4), 2336-2344.

De la O Serna, J. A. (2014). Synchrophasor measurement with polynomial phase-locked-loop Taylor–Fourier filters. IEEE Transactions on Instrumentation and Measurement, 64(2), 328-337.

De Sa, J. P., & Pedro, L. (1991). Modal Kalman filtering based impedance relaying. IEEE transactions on power delivery, 6(1), 78-84.

Derviškadić, A., Romano, P., & Paolone, M. (2017). Iterative-interpolated DFT for synchrophasor estimation: A single algorithm for P-and M-class compliant PMUs. IEEE Transactions on Instrumentation and Measurement, 67(3), 547-558.

Drummond, Z. D., Claytor, K. E., Allee, D. R., & Hull, D. M. (2020). An optimized subspace-based approach to synchrophasor estimation. IEEE Transactions on Instrumentation and Measurement, 70, 1-13.

Ferrero, R., Pegoraro, P. A., & Toscani, S. (2016). Dynamic fundamental and harmonic synchrophasor estimation by Extended Kalman filter. In 2016 IEEE International Workshop on Applied Measurements for Power Systems (AMPS) (pp. 1-6).

Fu, L., Yu, L., Xiong, S., He, Z., Mai, R., & Li, X. (2021). A dynamic synchrophasor estimation algorithm considering out-of-band interference. IEEE Transactions on Power Delivery, 37(2), 1193-1202.

Gökoğlu, A. (2019) Dördün genlik modülasyonu kullanarak senkrofazör ölçüm yöntemi (Master's thesis, Gazi Üniversitesi, Fen Bilimleri Enstitüsü).

Gurusinghe, D. R., Rajapakse, A. D., & Narendra, K. (2012, October). Evaluation of steady-state and dynamic performance of a synchronized phasor measurement unit. In 2012 IEEE Electrical Power and Energy Conference (pp. 57-62). IEEE.

Ipek, M. A. M. (2008) Elektrik güç sistemlerinde geniş alan ölçüm sistemi ve fazör ölçüm birimlerinin yerleştirilmesinin incelenmesi (Doctoral dissertation, Istanbul Teknik Üniversitesi, Fen Bilimleri Enstitüsü).

Jin, T., & Zhang, W. (2020). A novel interpolated DFT synchrophasor estimation algorithm with an optimized combined cosine self-convolution window. IEEE Transactions on Instrumentation and Measurement, 70, 1-10.

Liu, J., Ni, F., Pegoraro, P. A., Ponci, F., Monti, A., & Muscas, C. (2012, September). Fundamental and harmonic synchrophasors estimation using modified Taylor-Kalman filter. In 2012 IEEE International Workshop on Applied Measurements for Power Systems (AMPS) Proceedings (pp. 1-6).

Macii, D., Petri, D., & Zorat, A. (2012). Accuracy analysis and enhancement of DFT-based synchrophasor estimators in off-nominal conditions. IEEE transactions on Instrumentation and Measurement, 61(10), 2653-2664.

Moore, P. J., Carranza, R. D., & Johns, A. T. (1996). Model system tests on a new numeric method of power system frequency measurement. IEEE Transactions on Power Delivery, 11(2), 696-701.

Orallo, C. M., Carugati, I., Maestri, S., Donato, P. G., Carrica, D., & Benedetti, M. (2013). Harmonics measurement with a modulated sliding discrete Fourier transform algorithm. IEEE Transactions on Instrumentation and Measurement, 63(4), 781-793.

Premerlani, W., Kasztenny, B., & Adamiak, M. (2007). Development and implementation of a synchrophasor estimator capable of measurements under dynamic conditions. IEEE Transactions on Power Delivery, 23(1), 109-123.

Ren, J., & Kezunovic, M. (2011). Real-time power system frequency and phasors estimation using recursive wavelet transform. IEEE Transactions on Power Delivery, 26(3), 1392-1402.

Robbins, H.A, (2012). Circuit Analysis: Theory and Practice (5th ed.). Cengage Learning. p. 536. ISBN 978-1-285-40192-8.

Romano, P., & Paolone, M. (2014). Enhanced interpolated-DFT for synchrophasor estimation in FPGAs: Theory, implementation, and validation of a PMU prototype. IEEE Transactions on instrumentation and measurement, 63(12), 2824-2836.

Schweitzer, E. O., Whitehead, D., Zweigle, G., & Ravikumar, K. G. (2010, March). Synchrophasor-based power system protection and control applications. In 2010 63rd Annual Conference for Protective Relay Engineers (pp. 1-10).

Shan, X., Macii, D., Petri, D., & Wen, H. (2023). Enhanced ipd2ft-based synchrophasor estimation for m class pmus through adaptive narrowband interferers detection and compensation. IEEE Transactions on Instrumentation and Measurement, 73, 1-14.

Song, J., Zhang, J., Kuang, H., & Wen, H. (2022). Dynamic Synchrophasor Estimation Based on Weighted Real-Valued Sinc Interpolation Method. IEEE Sensors Journal, 23(1), 588-598.

Wood, H. C., Johnson, N. G., & Sachdev, M. S. (1985). Kalman filtering applied to power system measurements relaying. IEEE Transactions on Power Apparatus and Systems, (12), 3565-3573.

Zamora-Mendez, A., Paternina, M. R. A., Vázquez, E., Ramirez, J. M., & de Serna, J. A. L. O. (2015). Distance relays based on the Taylor–Kalman-Fourier filter. IEEE Transactions on Power Delivery, 31(3), 928-935.

Zhan, L., Liu, Y., & Liu, Y. (2016). A Clarke transformation-based DFT phasor and frequency algorithm for wide frequency range. IEEE Transactions on Smart Grid, 9(1), 67-77.

Zhang, P., Chen, J., & Shao, M. (2007). Phasor measurement unit (PMU) implementation and applications. Electr. Power Res. Inst. EPRI, Rep. Final 2007.

Zhao, W., Wang, L., & Zhang, Z. (2020). Artificial ecosystem-based optimization: a novel nature-inspired meta-heuristic algorithm. Neural Computing and Applications, 32(13), 9383-9425.